J. Fluid Mech. (2003), *vol.* 495, *pp.* 323–341.
DOI: 10.1017/S0022112003006268 Printed in the United Kingdom

The effect of numerical errors and turbulence models in large-eddy simulations of channel flow, with and without explicit filtering

By JESSICA GULLBRAND[1] AND FOTINI KATOPODES CHOW[2]

[1]Center for Turbulence Research, Stanford University, Building 500, Stanford, CA 94305-3030, USA
jes@ctr-sgi1.stanford.edu

[2]Environmental Fluid Mechanics Laboratory, Civil and Environmental Engineering, Stanford University, Terman Engineering Center M-13, Stanford, CA 94305-4020, USA
katopodes@stanfordalumni.org

(Received 12 November 2002 and in revised form 30 June 2003)

Turbulent channel flow simulations are performed using second- and fourth-order finite difference codes. A systematic comparison of the large-eddy simulation (LES) results for different grid resolutions, finite difference schemes, and several turbulence closure models is performed. The use of explicit filtering to reduce numerical errors is compared to results from the traditional LES approach. Filter functions that are smooth in spectral space are used, as the findings of this investigation are intended for application of LES to complex domains. Explicit filtering introduces resolved subfilter-scale (RSFS) as well as subgrid-scale (SGS) turbulence terms. The former can be theoretically reconstructed; the latter must be modelled. The dynamic Smagorinsky model, the dynamic mixed model, and the new dynamic reconstruction model are all studied. It is found that for explicit filtering, increasing the reconstruction levels for the RSFS stress improves the mean velocity as well as the turbulence intensities. When compared to LES without explicit filtering, the difference in the mean velocity profiles is not large; however the turbulence intensities are improved for the explicit filtering case.

1. Introduction

The equations for large-eddy simulation (LES) are obtained by applying a low-pass filter to the Navier–Stokes equations. This filtering operator divides the flow into so-called resolved and subfilter-scale (SFS) motions. When the equations are solved on a discrete grid, a discretization operator is applied to the equations as well, which further divides the turbulent flow field; the subfilter scales are divided into resolved SFS and unresolved SFS regions. The unresolved SFS motions are commonly called subgrid-scale motions (see also the notation used by Zhou, Brasseur & Juneja 2001). Figure 1 in § 2 depicts these regions of the flow field, which are described further later. The effect of the resolved subfilter-scale (RSFS) and subgrid-scale (SGS) motions on the resolved velocity field must be considered. The RSFS contribution can be theoretically reconstructed, and the SGS stress must be modelled. The filter shape as well as the filter width and, of course, the grid resolution are free parameters in LES.

For engineering purposes, second-order numerical methods are usually used when performing LES for complex flow fields. In LES the smallest resolved scales are often used to model the contribution from the unresolved scales. Therefore, it is of great importance that these small scales be resolved to high accuracy. High-accuracy LES results can be achieved by high-order numerical methods (see e.g. Morinishi *et al.* 1998) and/or by explicit filtering (Lund & Kaltenbach 1995). The complexity in implementing high-order methods as well as the computational cost become prohibitive when studying flow fields in complex geometries. Therefore, the use of explicit filtering may provide a favourable alternative.

In traditional LES solution methods, the computational grid and discretization operators are to be considered 'implicit' filtering of the Navier–Stokes equations. Using this approach, there is no need to define a filter function, but neither can the implicit filter be determined. The only actual filter that may be applied in the simulations is used in models for the RSFS and/or SGS contributions. One example is the need for a test filter in the dynamic Smagorinsky SGS model to determine the model coefficient.

In contrast, when explicit filtering is applied in LES, an explicitly defined filter function is needed. In this approach, the defined filter is used when calculating the RSFS contribution. If the dynamic Smagorinsky model (DSM) is used as the SGS model, an additional filter function (with larger width than the explicit filter) must also be defined for the test filter in the dynamic procedure. Both the RSFS and the SGS contributions must be included in the simulations. The differences in the implementation of the traditional LES and the explicitly filtered LES approaches might be considered subtle; however, the effect on the LES results is considerable.

The explicit filtering approach has recently been proposed as a method to minimize the influence of discretization error in finite difference codes (Lund & Kaltenbach 1995). All finite difference approximations have a truncation error that grows with increasing wavenumber. This truncation error can be reduced or eliminated when explicit filtering with a filter width larger than the computational grid cell size is applied (Lund 1997). Several researchers have investigated explicit filtering in turbulent channel flow. Lund & Kaltenbach (1995) used sharp cutoff filters (in spectral space) in the homogeneous directions with a second-order finite difference code (the same code used in this work). They concluded that the explicit filtering improved the accuracy of the LES results; however, mesh refinement without explicit filtering improved the results at a greater rate. All of their simulations used the DSM with a cutoff filter, which is not applicable to general geometries. Carati, Winckelmans & Jeanmart (2001) developed a useful framework for the explicit filtering approach. They proposed governing equations for LES which carefully distinguish between the discretization and filtering procedures. These equations are also used here to separate the RSFS and SGS effects used in explicit filtering. Winckelmans *et al.* (2001) performed simulations with explicit filtering using a fourth-order finite difference code (also used in this work). They applied second-order commutative filters in three dimensions, which introduce commutation errors in the wall-normal direction due to the stretched grid (Ghosal & Moin 1995). The explicit filtering approach (with low-order RSFS reconstruction) did not perform as well as DSM without explicit filtering (with a sharp cutoff test filter), though the authors suggested that higher-order reconstruction of the RSFS terms could improve the results obtained with explicit filtering. Gullbrand (2001) performed explicit filtering (also with low-order RSFS reconstruction) in three dimensions using commutative filters with the DSM in the same fourth-order finite difference code. Results without explicit filtering showed

better agreement with direct numerical simulation (DNS) data, also suggesting that higher-order reconstruction is needed for the RSFS terms.

In this investigation, we study the influence of numerical errors on the LES results, as well as the influence of the filtering approach and the reconstruction level on the turbulence models. The numerical error is studied by performing simulations of a turbulent channel flow using both second-order and fourth-order finite difference codes. The advantage of studying the channel flow is that both sharp cutoff and smooth filter functions can be used. In this work, the sharp cutoff filter is used only for comparison purposes, as our aims are to investigate approaches for LES over complex domains where sharp cutoffs cannot be used. The sharp cutoff is therefore used only for traditional LES, without explicit filtering. A smooth filter is applied for LES with explicit filtering. Higher-order reconstruction models for the RSFS stress are investigated with filters applied only in the homogeneous directions, as this avoids introducing commutation errors. The effect of three-dimensional filtering must ultimately be considered, but is left to future work. For turbulence models, the DSM, the dynamic mixed model (DMM), and the new dynamic reconstruction model (DRM) are all investigated. The DSM is used as the SGS model in all the simulations presented here. The DMM is a linear combination of the scale similarity model (SSM) of Bardina, Ferziger & Reynolds (1983), which acts as the RSFS model, and the DSM. In the DRM, the RSFS stress is modelled by using an estimate of the unfiltered velocity in the unclosed term; the SGS stress is again modelled by the DSM.

2. Governing equations

The governing equations for incompressible flow are the continuity equation together with the Navier–Stokes equations,

$$\frac{\partial u_i}{\partial x_i} = 0, \qquad \frac{\partial u_i}{\partial t} + \frac{\partial u_i u_j}{\partial x_j} = -\frac{\partial p}{\partial x_i} + \frac{1}{Re_\tau}\frac{\partial^2 u_i}{\partial x_j \partial x_j}. \tag{2.1}$$

Here u_i denotes the velocity, p pressure and Re_τ the Reynolds number based on the friction velocity and the channel half-width. Repeated indices indicate summation.

In computational LES, the governing equations are filtered in space and solved numerically on a grid. The traditional procedure for LES has been to treat the grid and the discretization operators as the filtering procedure of the governing equations. Here, we instead follow the approach of Carati *et al.* (2001) and Winckelmans *et al.* (2001) where the filtering and discretization procedures are treated separately. The discretization operator is represented by a tilde and the filtering operator by an overbar. The filter function G is applied to a flow variable f in physical space as

$$\overline{f}(x, \Delta, t) = \int_{-\infty}^{\infty} G(x, x', \Delta) f(x', t)\, \mathrm{d}x', \tag{2.2}$$

where Δ is the filter width. Thereby $\tilde{u}_i$ denotes a variable on the grid, and $\overline{\tilde{u}}_i$ denotes a filtered variable on the grid. Figure 1 shows a schematic of a typical energy spectrum from a turbulent flow. The spectrum can be separated into three parts (Carati *et al.* 2001; Zhou *et al.* 2001). The low-wavenumber portion is well-resolved on the grid, and is contained in the velocity $\overline{\tilde{u}}_i$. The shaded portion represents RSFS motions; this region contains filtered information that is still resolved on the grid. The subdomain between the dotted and solid lines is denoted the numerical error

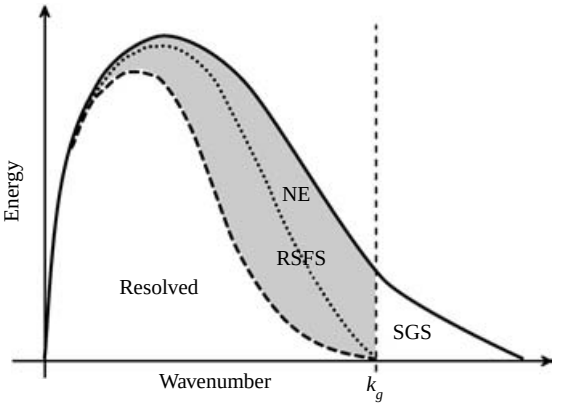

FIGURE 1. Schematic of velocity energy spectrum showing partitioning into resolved, subfilter-scale, and subgrid-scale motions. The numerical error region is also shown. The grid is indicated by the vertical dashed line, and the filter by the curved dashed line.

(NE) region, which is present due to the discretization errors. This region would not exist if spectral methods were used; in this particular case, the complete RSFS stress could be recovered. If numerical errors are present, the RSFS motions cannot be fully reconstructed. Finally, the high-wavenumber portion contains SGS motions that cannot be resolved on the grid, and must be modelled.

Hence, the LES momentum equations on a discrete mesh are written as

$$\frac{\partial \overline{\tilde{u}}_i}{\partial t} + \frac{\partial \widetilde{\overline{\tilde{u}}_j \overline{\tilde{u}}_i}}{\partial x_j} = \frac{\partial \overline{\tilde{p}}}{\partial x_i} + \frac{1}{Re_\tau} \frac{\partial^2 \overline{\tilde{u}}_i}{\partial x_j \partial x_j} - \frac{\partial \tilde{\tau}_{ij}}{\partial x_j} \tag{2.3}$$

where the turbulent stresses are defined as $\tau_{ij} = \overline{u_i u_j} - \overline{\tilde{u}}_i \overline{\tilde{u}}_j$. The filtered equations are not closed due to the nonlinear term $\overline{u_i u_j}$. Properties of the specific filters used are described in §4. Note that each term in the equation contains the effects of discretization, denoted by the tilde operator. In a spectral code, the effect of the discretization is simply a spectral cutoff filter, where the discretization and filtering operators clearly commute (i.e. $\tilde{\overline{u}} = \overline{\tilde{u}}$). (Note that the cutoff filter is more accurately termed a 'cutoff projection', as it is not reversible. However, we use the term 'cutoff filter' as is commonly done in the literature.) With finite differences, each term in the governing equations is affected differently by the discretization. The modified wavenumber effect (Moin 2001) will damp motions near the grid cutoff, as indicated in the NE region of figure 1. Thus the discretization acts as a smooth filter that is applied to the flow fields (though the exact nature of this smooth filter is unknown). In this work, we also assume $\tilde{\overline{u}} = \overline{\tilde{u}}$ when finite differences are used. When simulations are performed using the actual LES code, numerical errors due to the space and time discretization schemes will interact, making the effects of explicit spatial filtering and the grid cutoff filter impossible to separate. Conceptually, however, figure 1 serves to separate these effects so that we can address each as is appropriate.

Following Carati *et al.* (2001), the turbulent stresses can be separated into two parts, $\tau_{ij} = B_{ij} + \overline{A}_{ij}$, where

$$B_{ij} = \overline{\tilde{u}_i \tilde{u}_j} - \overline{\tilde{u}}_i \overline{\tilde{u}}_j, \qquad \overline{A}_{ij} = \overline{u_i u_j} - \overline{\tilde{u}_i \tilde{u}_j}. \tag{2.4}$$

$\overline{A}_{ij}$, which we call the SGS stress, depends on scales beyond the resolution domain of the LES. B_{ij}, the RSFS stress, depends on the differences between the exact and

filtered velocity fields within the resolution domain. As the filter width increases, the total turbulent stress term, consisting of the SGS and RSFS terms, will increase. The RSFS component can be computed theoretically, as an infinite expansion in a series model for $\tilde{u}_i$ would give the exact form (Yeo & Bedford 1988; Katopodes, Street & Ferziger 2000; Stolz, Adams & Kleiser 2001). Further discussion concerning partitioning of the RSFS and the SGS stresses can be found in Carati *et al.* (2001) and Winckelmans *et al.* (2001).

3. Resolved subfilter-scale and subgrid-scale models

When an explicit filter is applied to the Navier–Stokes equations, as in (2.3) above, information at the high wavenumbers is damped. In theory, this RSFS information can be restored exactly by using an inverse filtering operation. Several methods have been proposed to approximate this inverse filtering operation. Stolz *et al.* (2001) use the van Cittert (1931) iterative method in their approximate deconvolution procedure to reconstruct the unfiltered velocity field $\tilde{u}_i$ from the filtered field $\overline{\tilde{u}}_i$. Chow & Street (2002) use Taylor series expansions to obtain the unfiltered velocity. These unfiltered fields, $\tilde{u}_i$, are then substituted into the expression for B_{ij} to obtain the RSFS reconstruction. The SSM (Bardina *et al.* 1983) and the tensor-diffusivity model (Leonard 1974) can be derived from either of these reconstruction procedures by truncating the series expansions after a specified number of terms (Katopodes *et al.* 2000; Winckelmans *et al.* 2001). By truncating these series, a model is obtained for the RSFS term B_{ij}. However an additional stress term ($\overline{A}_{ij}$) is still required to model the SGS stresses. Note that if the problem domain can be transformed into spectral space, the filter (if it is smooth) can be exactly inverted, and an exact reconstruction can be obtained. Explicit filtering is thus of no advantage for reducing numerical errors when smooth filters are used in spectral methods (Winckelmans & Jeanmart 2001). If higher-order finite difference schemes are used, explicit filtering to reduce numerical errors may also become less important.

In this study, both low-order (the SSM) and higher-order reconstructions (obtained with the van Cittert iterative method) are used to model the RSFS stresses. In order to make a fair comparison between the RSFS models, the same SGS model (DSM) is used in all the simulations. The combinations of RSFS and SGS models used are described below. Tests without explicit filtering are also performed for comparison purposes.

3.1. *Dynamic Smagorinsky model* (*DSM*)

The DSM is a widely used eddy-viscosity SGS model (Smagorinsky 1963):

$$\tau_{ij} = -2\tilde{\nu}_e \overline{\tilde{S}}_{ij} = -2(C\tilde{\Delta})^2 |\overline{\tilde{S}}| \overline{\tilde{S}}_{ij}, \tag{3.1}$$

where ν_e is the eddy viscosity, $\tilde{\Delta}$ the effective grid cell spacing and S_{ij} the strain rate tensor. The exact definition of $\tilde{\Delta}$ is not needed as the total model parameter $C\tilde{\Delta}$ is calculated dynamically (Germano *et al.* 1991) using the least-squares approximation of Lilly (1992). The choice of the explicit filter and the test filter for the dynamic procedure greatly affects the performance of the DSM, as discussed further below. The DSM is used in our simulations with and without explicit filtering.

3.2. *Dynamic mixed model* (*DMM*)

Low-order reconstruction of the RSFS stresses can be obtained by using the scale-similarity model proposed by Bardina *et al.* (1983). The SSM can be derived by

substituting $\tilde{u}_i \approx \overline{\tilde{u}}_i$ into the definition of the RSFS stress tensor, B_{ij}. Here the RSFS stress is modelled by the scale-similarity term and the DSM is used as the SGS model, in a procedure similar to that of Vreman, Geurts & Kuerten (1994):

$$\tau_{ij} = \overline{\overline{\tilde{u}}_i \overline{\tilde{u}}_j} - \overline{\overline{\tilde{u}}_i}\,\overline{\overline{\tilde{u}}_j} - 2(C\tilde{\Delta})^2 |\overline{\tilde{S}}| \overline{\tilde{S}}_{ij}, \tag{3.2}$$

where the contribution of the SSM is taken into account in the calculation of the dynamic coefficient. In addition, the test and explicit filters must be carefully applied in the dynamic procedure, leading to a different form of the test-filtered equations, as described by Winckelmans *et al.* (2001). The SSM term is discretized with the same method as the convective term in each code.

3.3. *Dynamic reconstruction model* (*DRM*)

Higher-order reconstruction of the RSFS stress tensor can be achieved by the iterative deconvolution method of van Cittert (1931). The unfiltered quantities can be derived by a series of successive filtering operations (G) applied to the filtered quantities with

$$\tilde{u}_i = \overline{\tilde{u}}_i + (I - G) * \overline{\tilde{u}}_i + (I - G) * ((I - G) * \overline{\tilde{u}}_i) + \cdots \tag{3.3}$$

where I is the identity matrix. The truncation order of the expansion determines the level of deconvolution, as discussed by Stolz *et al.* (2001). Level-n reconstruction includes the first $n + 1$ terms of the series.

The series expansion provides an estimate for the inversion of the filter G. If G is positive in Fourier space for all wavenumbers, the exact inverse can be obtained by simply inverting the filter kernel in wave space. If G crosses from positive to negative values in wave space at any wavenumber, exact inversion becomes impossible due to division by zero. Therefore, the series reconstruction over all wavenumbers of such a filtered field is approximate. The exact reconstruction can only be obtained as long as the filter kernel is positive in wave space. Hence, it is preferable to choose an explicit filter function that is positive for at least all the wavenumbers that are represented in the simulation (see figure 2 in § 4 below for the filters used in this work).

The approximate unfiltered velocity, $\tilde{u}_i^\star$ (due to the truncated series), is substituted into the first term ($\overline{\tilde{u}_i \tilde{u}_j}$) of the RSFS stress which becomes $\overline{\tilde{u}_i^\star \tilde{u}_j^\star}$. This reconstruction was used by Stolz *et al.* (2001) who called the RSFS model the approximate deconvolution model (ADM). Here the ADM is used together with the DSM:

$$\tau_{ij} = \overline{\tilde{u}_i^\star \tilde{u}_j^\star} - \overline{\tilde{u}}_i \overline{\tilde{u}}_j - 2(C\tilde{\Delta})^2 |\overline{\tilde{S}}| \overline{\tilde{S}}_{ij}, \tag{3.4}$$

which we call the dynamic reconstruction model (DRM). The ADM portion of the DRM is discretized with the same method as the convective term. The ADM with the DSM was also independently proposed and used as a model by Winckelmans & Jeanmart (2001) for isotropic decaying turbulence. Reconstruction series of level five and ten are used in this study and they are denoted DRM5 and DRM10, respectively.

4. Filter functions

In finite difference methods, the filter in the LES equations is important for limiting numerical errors. As shown by Ghosal (1996) and Chow & Moin (2003), numerical errors from finite difference schemes can be larger than the entire contribution from the turbulence closure term, $\partial \tau_{ij}/\partial x_j$. To avoid this problem, the explicit filter width should be at least twice as large as the cell size for a fourth-order-accurate finite difference code. For a second-order finite difference code, these studies suggest that the filter width should be four times the cell size. In this work, the filter width in the

case of the second-order code is not four times the cell size, but instead is chosen to be the same as the one used in the fourth-order code. The effect of this choice on the results warrants further study.

The correct use of the filter is especially important in the RSFS stress models, particularly in the dynamic procedure which is based on the scale-similarity assumption in the Germano identity (Germano *et al.* 1991). To compute a quantity such as $\widehat{\overline{\tilde{u}}_i}$ in the dynamic procedure, the test filter ('caret' symbol) must be explicitly applied. To satisfy scale-similarity, it is required that the hat operator be 'similar' to the overbar operator. Therefore, if the filtering operator (the overbar) is a tophat, the combined effect of the two (caret and overbar) should also be a tophat filter. Such an operator can be obtained by following the method of Carati *et al.* (2001) and Winckelmans *et al.* (2001), described below.

A discrete approximation to a tophat filter of twice the cell size can be obtained by trapezoidal rule integration. In one dimension the filter is

$$\overline{\phi}_i = 0.25\phi_{i-1} + 0.5\phi_i + 0.25\phi_{i+1}. \tag{4.1}$$

However, the effective filter width of this discrete filter is no longer twice the cell size, but rather $\sqrt{6}$. If Simpson's rule were used to derive a discrete version of the tophat filter, the weights would instead be $(1/6, 2/3, 1/6)$, with an effective filter width of twice the cell size. Despite the inconsistency in the effective filter width for (4.1), this filter was chosen because the function goes to zero (in spectral space) at the grid cutoff and therefore eliminates the highest wavenumber that could be sustained by the grid (see e.g. Najjar & Tafti 1996).

To construct an appropriate test filter, it is useful to write the tophat filter in Fourier space as $\overline{G}(k) = \sin(k\Delta)/(k\Delta)$. The combined effect of the test filter (at twice the width) and the explicit filter (the overbar) should thus also be a tophat: $\widehat{\overline{G}}(k) = \sin(2k\Delta)/(2k\Delta)$. The required test filter (acting alone), would therefore be

$$\hat{G}(k) = \sin(2k\Delta)/(2\sin(k\Delta)) = \cos(k\Delta). \tag{4.2}$$

If we now transform this back into physical space, we have a discrete filter which requires only the immediate neighbouring values,

$$\hat{\phi}_i = 0.5\phi_{i-1} + 0.5\phi_{i+1}. \tag{4.3}$$

The combined effect of the overbar and hat filters in physical space is also a tophat, but over a wider grid stencil, as expected:

$$\widehat{\overline{\phi}}_i = 0.125\phi_{i-2} + 0.25\phi_{i-1} + 0.25\phi_i + 0.25\phi_{i+1} + 0.125\phi_{i+2}. \tag{4.4}$$

The filter functions are plotted in figure 2. Note that $\widehat{\overline{G}}$ becomes negative over the upper half of the resolved wavenumber region. To guarantee similarity between $\widehat{\overline{G}}$ and $\overline{G}$ this test filter should in fact be accompanied by a sharp cutoff filter at half the Nyquist frequency so that these negative values are set to zero. This sharp cutoff filter is indicated by $\tilde{u}^c$ in the dynamic procedure described by Winckelmans *et al.* (2001) where c indicates the cutoff filter at the coarser resolution of the test filter. In the implementation of the dynamic procedure used in this paper, this coarse cutoff filter has not been explicitly applied as it is not practical for complex geometries; simulations performed with or without the coarse cutoff filter showed no discernable differences.

In this investigation, the same tophat explicit and test filters are used in both the second- and fourth-order finite difference codes. The explicit and test filters are

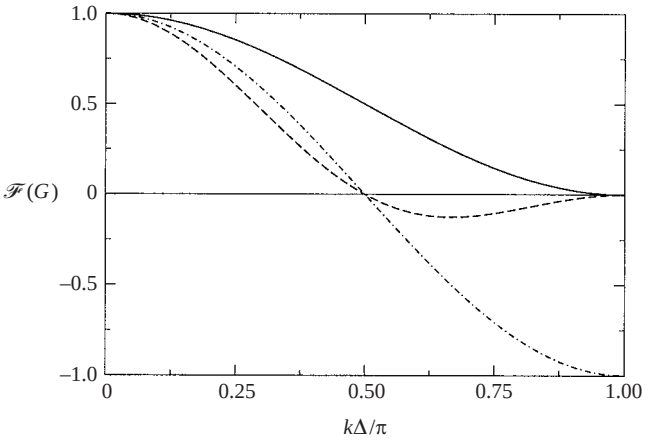

FIGURE 2. Fourier transforms of the explicit and test filters, shown in one dimension. The explicit filter (———) goes to zero at $k = \pi/\Delta x$ (the Nyquist wavenumber). The effective test filter (– – – –) is generated by applying the test filter (—·—) to the explicit filter; the resulting filter crosses zero at $k = \pi/2\Delta x$.

applied only in the homogeneous directions, as is commonly done in channel flow studies. Though this choice is not entirely self-consistent, it allows a direct comparison between the second- and fourth-order LES codes without introducing commutation errors due to filtering in the wall-normal direction over a stretched grid (Gullbrand 2001). Note that the test filter in (4.3) is only used in the simulations with explicit filtering, as done by Winckelmans *et al.* (2001). When no explicit filter is applied, the tophat in (4.1) is used as the test filter. Also note that in the finite difference codes, for both the explicit filtering and the traditional approaches, the filters are applied only in calculations of the RSFS or SGS terms, and do not appear elsewhere in the code.

5. Solution algorithm

The second- and fourth-order codes represent spatial derivatives on staggered grids with second- and fourth-order central difference schemes, respectively. In the second-order code, the convective terms are discretized in divergence form, while in the fourth-order code, they are in skew-symmetric form (Morinishi *et al.* 1998; Vasilyev 2000). In both codes, the equations are integrated in time using the third-order Runge–Kutta scheme described by Spalart, Moser & Rogers (1991). The diffusion terms in the wall-normal direction are treated implicitly with the Crank–Nicolson scheme. The splitting method of Dukowicz & Dvinsky (1992) is used to enforce the solenoidal condition. The resulting discrete Poisson equation for the pressure is solved in the wall-normal direction using a tri-diagonal direct matrix solver in the second-order code and a penta-diagonal matrix solver in the fourth-order code. In the homogeneous directions, the Poisson equation is solved using a discrete Fourier transform in both codes. Periodic boundary conditions are applied in the streamwise and spanwise homogeneous directions, with no-slip conditions at the channel walls. A fixed mean pressure gradient is used to drive the flow. The Reynolds number is $Re_\tau = 395$ and the computational domain is $(2\pi h, 2h, \pi h)$ in (x, y, z) where x is the streamwise direction, y the wall-normal direction, and z the spanwise direction. The

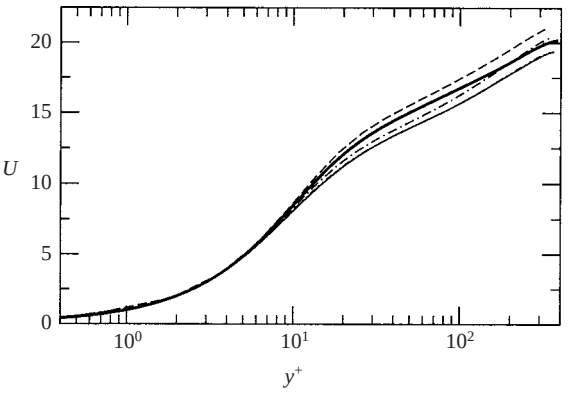

FIGURE 3. Mean velocity profiles for different grid sizes for the second-order code using no turbulence model: – – – –, 48,37,36; —·—, 64,49,48; —··—, 81,65,64; ———, 96,73,72; and ———, DNS.

computational grid is stretched in the y-direction by a hyperbolic tangent function

$$y(j) = -\frac{\tanh(\gamma(1-2j/N_2))}{\tanh(\gamma)}, \qquad j = 0, \ldots, N_2, \tag{5.1}$$

where N_2 is the number of grid points in the wall-normal (j) direction and γ is the stretching parameter, which is set to 2.75. The computational codes are compared in Gullbrand (2000).

6. Turbulent channel flow simulations

6.1. *Effect of grid resolution and numerical error*

As one focus of this work is to examine the effect of numerical errors in actual LES, two finite difference codes (one second-order and one fourth-order) are used. Because of the difference in accuracy between the codes, the grid resolution needs to be chosen carefully for a better comparison of the results. Figure 3 shows the effect of increasing grid resolution for the second-order code, using no turbulence closure model. All results are compared to DNS data obtained using the fourth-order finite difference code (using no turbulence model) and the same grid resolution (256,193,192) used by Moser, Kim & Mansour (1999) for their DNS calculations. (The DNS statistics from the fourth-order code were found to be virtually identical to the spectral code DNS data of Moser *et al.* (1999).) It is clear that the choice of resolution can significantly alter the results of the simulation. The results in figure 3 show a minimum grid resolution of (81,65,64) where the results do not seem to be greatly affected by the numerical errors. This should be one of the necessary criteria in order to determine the required grid resolution. Of course as the grid resolution is increased the solution will eventually approach the DNS results. Due to increased accuracy (compared to the second-order code), the required minimum resolution for the fourth-order code is coarser at (64,49,48).

It is expected that for a given resolution, the performance of the fourth-order code will be better than the second-order code, due to the higher accuracy of the finite difference schemes. Figure 4 shows results of simulations made with the same grid resolution (48,37,36) for both finite difference codes and for the pseudo-spectral code of Jeanmart & Winckelmans (2002). The pseudo-spectral code uses fourth-order

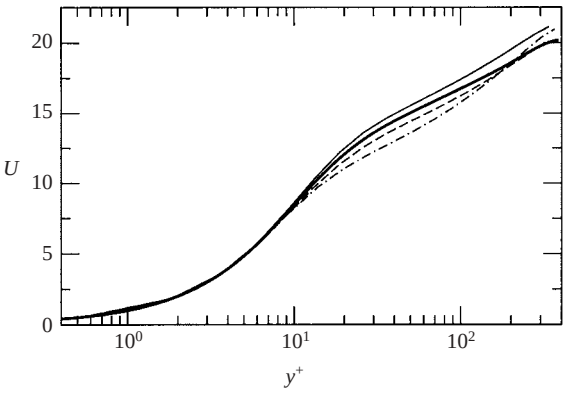

FIGURE 4. Mean velocity profiles for three different LES codes with the same grid resolution (48,37,36) using no turbulence model: ———, second-order; – – – –, fourth-order; —·—, pseudo-spectral; ▬▬, DNS.

compact finite differences in the vertical direction and is spectral in the horizontal directions. The simulations are performed without a closure model, so that the effect of the numerical errors can be compared. As seen in figure 3, increasing resolution (and hence decreasing numerical errors) first reduces the mass flow predicted (mean velocity profile) in the simulations to a level lower than the DNS results. If the resolution is further increased, the mass flow increases and approaches the DNS results from below. Similarly, it is expected that for a given grid resolution, the pseudo-spectral code will produce the lowest mean velocity profile of the three codes, as it has the lowest numerical errors (see figure 4). The fourth-order finite difference code also predicts a mean velocity profile that is lower than the DNS for this resolution (but higher than the pseudo-spectral code); however the second-order code does not, due to the effect of large truncation errors.

Because of the large differences in the profiles in figure 4, different grid resolutions are chosen for each finite difference code to compare results fairly in further tests. In this way, we attempt to minimize the numerical differences at the outset of the investigation, though the interaction of these errors with different RSFS and SGS models is still an issue. To choose the appropriate resolution, simulations with the DSM using a spectral cutoff test filter with a width of twice the grid cell size were performed at different resolutions until good agreement was obtained. (Agreement at the two chosen resolutions can be seen in figures 5 and 6, as described later.) We use the cutoff filter case as the base case for comparison because this approach does not involve explicit filtering and thus provides an independent reference.

The grid resolutions for the remaining simulations are therefore as follows. The fourth-order finite difference code resolution is chosen to be (64,49,48), which is one quarter of the DNS resolution in each spatial direction. This resolution corresponds to a streamwise grid cell size of $\Delta x^+ = 39$, and a spanwise cell size of $\Delta z^+ = 26$. Non-dimensional 'plus' units are defined as $y^+ = yu_\tau/\nu$, where u_τ is the friction velocity and ν is the kinematic viscosity. The range of the cell size in the wall-normal direction is $0.4 \leqslant \Delta y^+ \leqslant 45$. In the simulations using the second-order code, a grid resolution of (81,65,64) is employed. This resolution corresponds to $\Delta x^+ = 31$, $\Delta z^+ = 19$ and $0.3 \leqslant \Delta y^+ \leqslant 34$. Thus the choice of grids for each code corresponds to the grid size which was shown to not be greatly influenced by the numerical errors for the 'no model' tests mentioned previously. The time step used is 1.5×10^{-3} and is the same

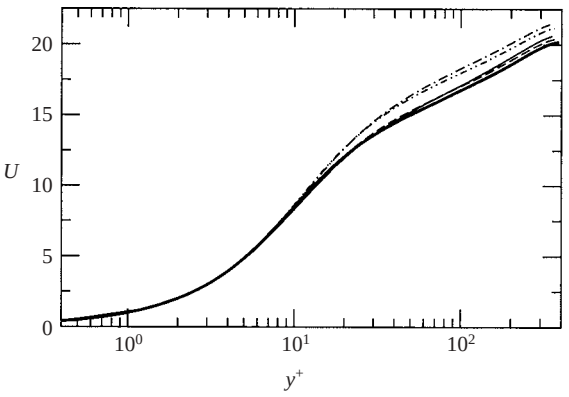

FIGURE 5. Mean velocity profiles for the second-order (81,65,64) and fourth-order (64,49,48) codes without explicit filtering: ———, fourth-order code, DSM with sharp cutoff filter; – – – –, second-order code, DSM with sharp cutoff filter; —·—, fourth-order code, DSM with tophat filter; —··—, second-order code, DSM with tophat filter; and ———, DNS.

in both codes. A statistically stationary solution is obtained after 30 dimensionless time units and thereafter statistics are sampled during 15 time units. The time is normalized with the friction velocity and the channel half-width.

6.2. *SGS modelling: LES without explicit filtering*

For the purpose of comparison, tests are performed using traditional SGS model formulations. These simulations do not use explicit filtering, meaning that the only filter that is actually applied is the test filter in the dynamic procedure, and this is chosen to be twice the cell size. In our test cases without explicit filtering, the reconstruction term (the RSFS stress) is not considered; only the SGS stress is modelled. By using the tophat filter (which is smooth in spectral space) as the test filter in the dynamic procedure (see below), it is assumed that the implicit filter is also a tophat; therefore the RSFS stress should in theory be considered. However, the implicit filter cannot be determined, meaning that reconstruction of the RSFS stress is questionable.

For the channel flow, the lateral periodic boundary conditions allow the use of a spectral cutoff filter for the test filter. It is well known (Piomelli, Moin & Ferziger 1988) that the Smagorinsky model performs best when used together with such a cutoff filter. The difficulty with this filter choice is that it cannot be easily applied to other geometries. The cutoff filter width in our simulations is twice the cell size, giving the filter–grid ratio $\alpha = \Delta/\Delta_g = 2$, where Δ and Δ_g are the filter width and grid cell size respectively. Because filtering is only applied in the x- and z-directions, the effective filter–grid ratio squared is $\alpha_{eff}^2 = 4^{2/3}$. Simulations with the DSM using a tophat filter in physical space as the test filter are also performed. The test filter is applied as in (4.1); the filter–grid ratio in this case is $\alpha = \sqrt{6}$ and hence $\alpha_{eff}^2 = 6^{2/3}$ (see Najjar & Tafti 1996; Lund 1997).

Figure 5 shows mean velocity profiles from both the second- and fourth-order finite difference codes, compared with DNS data. Agreement between the second- and fourth-order codes for the simulations using the cutoff filter is quite good, indicating that the chosen resolution for each code is good for comparisons. The agreement between the second- and fourth-order codes for the reduced (deviatoric) turbulence intensities for the cutoff filter case is excellent, as seen in figure 6. The turbulence intensities are adjusted by removing the trace from each tensor component,

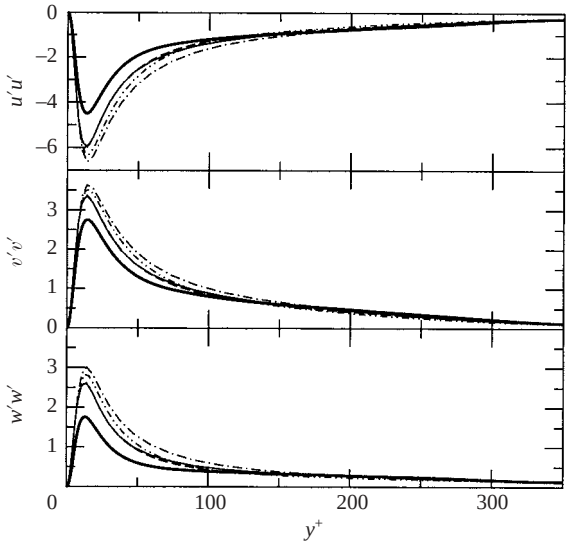

FIGURE 6. Profiles of reduced turbulence intensities in streamwise $u'u'$, wall normal $v'v'$ and spanwise $w'w'$ directions for the second-order (81,65,64) and fourth-order (64,49,48) codes without explicit filtering. The trace is removed from each tensor component. ———, fourth-order code, DSM with sharp cutoff filter; – – – –, second-order code, DSM with sharp cutoff filter; —·—, fourth-order code, DSM with tophat filter; —··—, second-order code, DSM with tophat filter; and ———, DNS.

as discussed by Winckelmans, Jeanmart & Carati (2002). Results for the tophat filter are, as expected, worse than for the spectral cutoff filter. This is due to the absence of the RSFS component of the total stress, which should be present when a smooth filter is applied, as discussed further below. Though it is known to perform poorly with a smooth filter, the DSM is frequently used with the tophat filter because spectral cutoff filters cannot be applied in domains with general geometries. Note that the profiles obtained by the second-order code in figures 5 and 6 are slightly closer than the fourth-order code to the DNS for the tophat filter cases, which is due to the choice of higher resolution for this code than the fourth-order code. Tests performed using the same resolution (64,49,48) for both codes showed that the results from the fourth-order code are closer to the DNS data than are the results from the second-order code. This is expected based on the visible effect of numerical errors in the comparisons of the codes using no turbulence model, shown in figure 4, and as discussed previously in the choice to use different resolutions for each code.

Profiles of the SGS stress $\tilde{\tau}_{12}$ over half the channel width are shown in figures 7 and 8 for the fourth- and second-order codes, respectively. The contribution of the SGS stress is smaller for the second-order code because the simulations are performed using a higher resolution, meaning that more of the turbulent motions are resolved. The SGS stress is larger for the tophat filter cases for both codes because the effective filter width of the tophat is larger ($\sqrt{6}$ compared to 2), which therefore places more energy into the SGS terms. The predicted SGS stresses are compared to the SGS contribution calculated from the filtered DNS velocity data. The SGS stress tensor ($\tilde{\tau}_{ij} = \widetilde{u_i u_j} - \tilde{u}_i \tilde{u}_j$) is calculated *a posteriori* assuming the implicit filter is a sharp cutoff filter. The cutoff filters for filtering the DNS data are chosen separately to correspond to the two grid resolutions used: the (64,49,48) grid used for the fourth-order LES

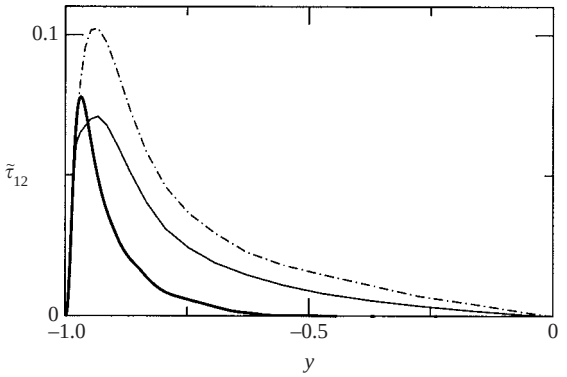

FIGURE 7. Profiles of the turbulent stress $\tilde{\tau}_{12}$ for the fourth-order (64,49,48) code without explicit filtering: ———, DSM with sharp cutoff filter; —·—, DSM with tophat filter; ———, DNS.

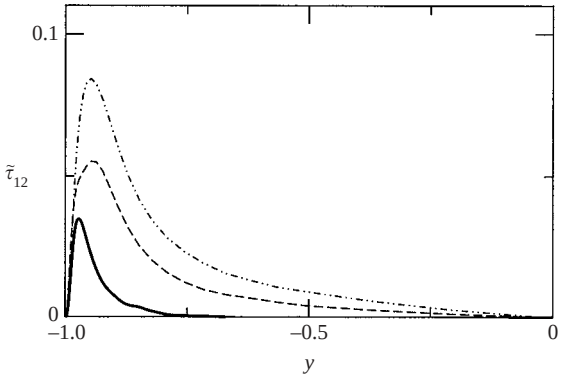

FIGURE 8. Profiles of the turbulent stress $\tilde{\tau}_{12}$ for the second-order (81,65,64) code without explicit filtering: – – – –, DSM with sharp cutoff filter; —··—, DSM with tophat filter; ———, DNS.

calculations, and the (81,65,64) grid used for the second-order code. No filters are applied in the vertical direction. The filtered DNS results for $\tilde{\tau}_{12}$ shown in figures 7 and 8 do not provide a clear indication of the performance of the LES simulations. This poor agreement is probably due to the assumption of using a sharp cutoff filter in the DNS calculation of $\tilde{\tau}_{12}$. The actual implicit filter cannot be determined, but is probably closer to a smooth filter function since it is affected by finite difference errors (due to the modified wavenumber effect).

6.3. *RSFS and SGS modelling: LES with explicit filtering*

To attempt to minimize the influence of discretization errors in finite difference or finite volume codes, explicit filtering can be used. The difference between the implementation of this approach and that of § 6.2 is in the filters used in the closure models, and thus the ability to reconstruct the RSFS terms. As this approach is geared toward finite difference methods in complex domains, the filters used must be smooth; the spectral cutoff filter is not used here in this approach.

We performed several simulations using explicit filtering with increasing levels of reconstruction for the RSFS stresses. For the first case, the DSM is applied using an explicit filter of width twice the grid cell size and a test filter of four times the cell

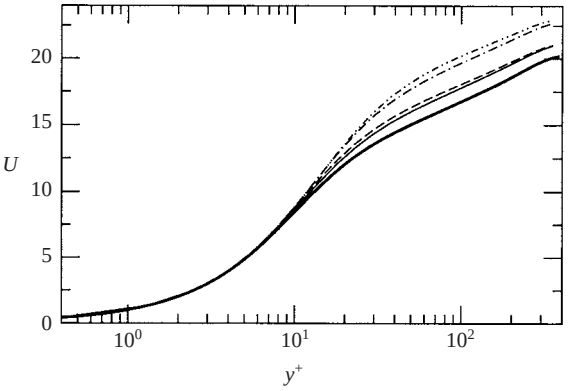

FIGURE 9. Mean velocity profiles for the fourth-order code (64,49,48) with explicit filtering (tophat) and reconstruction: —··—, DSM; —·—, DMM; – – – –, DRM5; ———, DRM10; and ———, DNS.

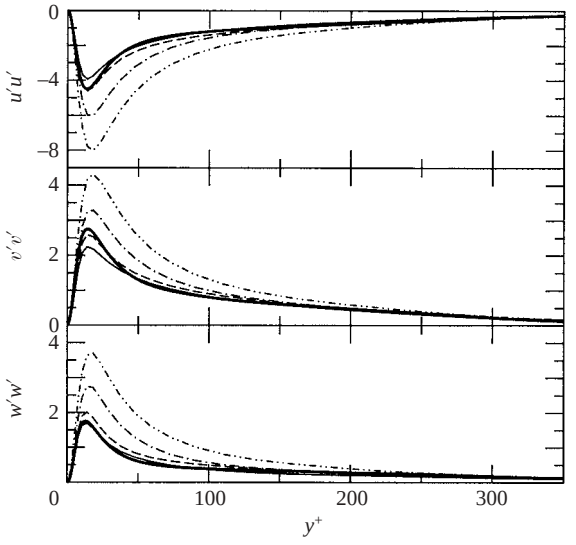

FIGURE 10. Profiles of reduced turbulence intensities in streamwise $u'u'$, wall normal $v'v'$ and spanwise $w'w'$ directions for the fourth-order (64,49,48) code with explicit filtering (tophat) and reconstruction. The trace is removed from each tensor component. —··—, DSM; —·—, DMM; – – – –, DRM5; ———, DRM10; and ———, DNS.

size. The effective filter ratio for the dynamic procedure is chosen to be 2, as done by Winckelmans *et al.* (2001); the determination of the optimal ratio is left to further investigations. This first case has no reconstruction terms. Then, reconstruction to the first level is added by using the DMM, followed by the DRM5 and DRM10 with five and ten levels of reconstruction, respectively (see §§ 3.2 and 3.3). Figure 9 shows that the mean velocity profiles for the fourth-order code improve compared to the DNS results as the level of reconstruction increases. The improvement is very clear in the comparison of the reduced turbulence intensities in figure 10. However, the incremental improvement between DRM5 and DRM10 is not large, indicating that good reconstruction of the unfiltered velocity is most likely already obtained by DRM5. The differences between the LES results (with DRM5 and DRM10) and the DNS results are therefore most probably due to numerical errors (see the NE

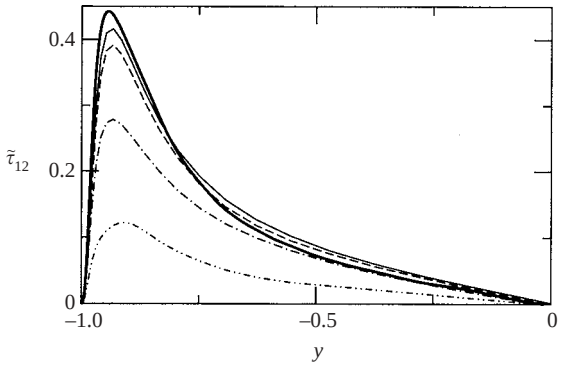

FIGURE 11. Profiles of the turbulent stress $\tilde{\tau}_{12}$ for the fourth-order (64,49,48) code with explicit filtering (tophat) and reconstruction: —··—, DSM; —·—, DMM; - - - -, DRM5; ———, DRM10; and ———, DNS.

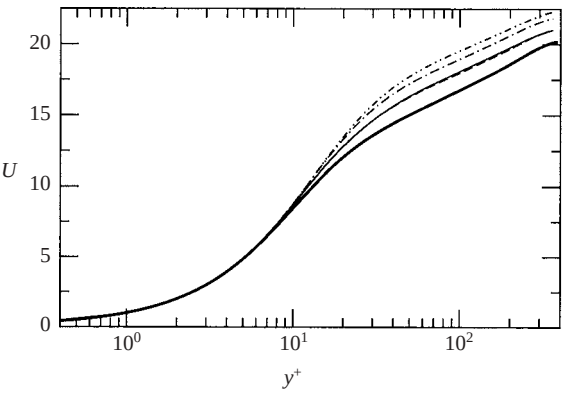

FIGURE 12. Mean velocity profiles for the second-order code (81,65,64) with explicit filtering (tophat) and reconstruction: —··—, DSM; —·—, DMM; - - - -, DRM5; ———, DRM10; and ———, DNS.

region in figure 1) and the SGS model used. The total turbulent stress $\tilde{\tau}_{12}$ shown in figure 11 increases considerably with increasing reconstruction level (though only slightly between DRM5 and DRM10). For each case, the contribution of the DSM portion (not shown) of the model is roughly the same, with a peak of around 0.1, so the increase of the modelled stresses is almost entirely due to the RSFS model. The turbulent stresses are compared to DNS values calculated by using the definition of the turbulent stress tensor ($\tilde{\tau}_{ij} = \widetilde{u_i u_j} - \tilde{\bar{u}}_i \tilde{\bar{u}}_j$). The DNS fields are obtained using the fourth-order code as described previously in § 6.2. The discrete quantities $\tilde{u}_i$ are obtained from the DNS fields *a posteriori* by using a sharp cutoff filter chosen to match the grid resolution used by the second- (81,65,64) and fourth-order (64,49,48) LES simulations. The explicit filter is then twice the corresponding LES cell spacing; for each grid size a tophat filter is constructed using the trapezoidal rule for the DNS fields to match the filter width used in each LES simulation. No filters are applied in the vertical direction. The turbulent stresses predicted by the DRM show very good agreement with the stresses calculated from the DNS data. Results for the second-order code are shown in figures 12 and 13. Turbulence intensities are not shown for the second-order code as the pattern of improvement is similar to that of the fourth-order code.

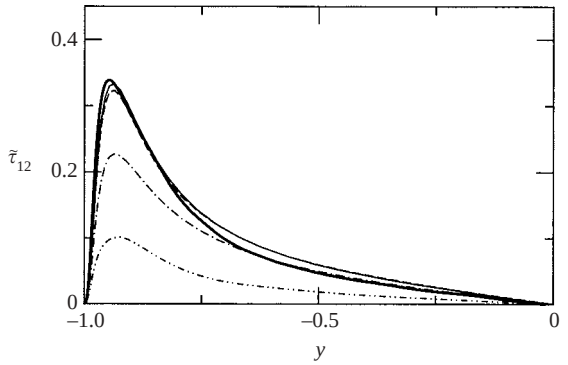

FIGURE 13. Profiles of the turbulent stress $\tilde{\tau}_{12}$ for the second-order (81,65,64) code with explicit filtering (tophat) and reconstruction: —··—, DSM; —·—, DMM; – – – –, DRM5; ———, DRM10; and ▬▬, DNS.

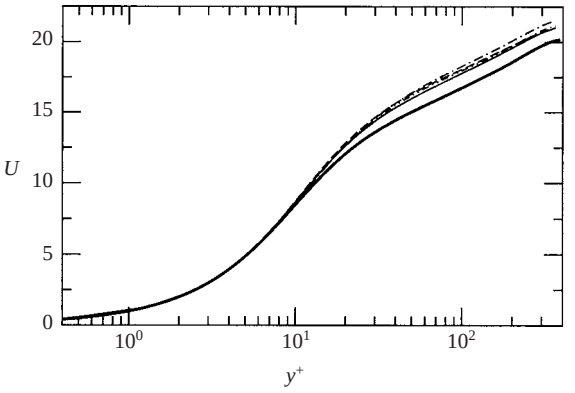

FIGURE 14. Mean velocity profiles for the second-order (81,65,64) and fourth-order (64,49,48) codes with and without explicit filtering (using tophat filters for both): ———, fourth-order code, DRM10; – – – –, second-order code, DRM10; —·—, fourth-order code, DSM no explicit filtering; —··—, second-order code, DSM no explicit filtering; and ▬▬, DNS.

7. Discussion and conclusions

Despite the existing theory and previous attempts at LES using explicit filtering (Carati *et al.* 2001; Winckelmans *et al.* 2001; Lund & Kaltenbach 1995), the advantages of this method in practice remain unclear. Because of the extra filtering operations, the explicit filtering approach is necessarily more computationally expensive than traditional LES. However, explicit filtering offers the potential to limit the influence of numerical errors from finite difference schemes on the flow solution.

Figure 14 compares results from both the second- and fourth-order codes, with and without explicit filtering. The models used are the DSM with the tophat filter (without explicit filtering, as is common in engineering applications) and the DRM10 (with explicit filtering). For both codes, there are only slight differences in the mean flow profiles for the cases with and without explicit filtering. The largest difference is seen in the reduced turbulence intensities, shown in figure 15, where the improvements due to DRM10 are quite significant. Even the magnitudes of the reduced streamwise intensities $u'u'$ for DRM10 are smaller than the DNS values, which is the opposite of what is usually observed with turbulence closures such as the DSM (Gullbrand

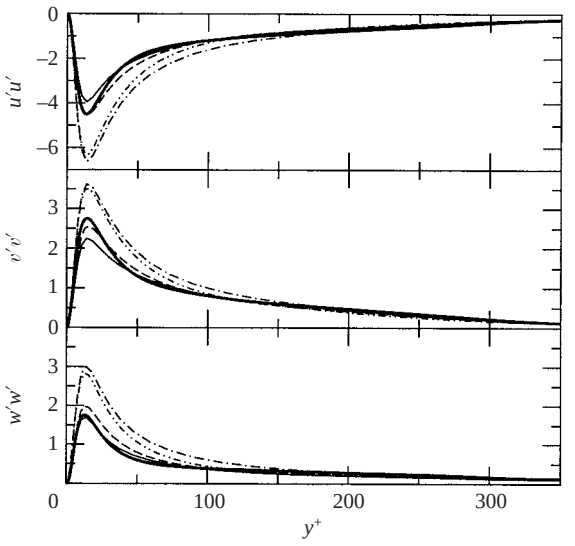

FIGURE 15. Profiles of reduced turbulence intensities in streamwise $u'u'$, wall normal $v'v'$ and spanwise $w'w'$ directions for the second-order (81,65,64) and fourth-order (64,49,48) codes with and without explicit filtering (using tophat filters for both). The trace is removed from each tensor component. ——, fourth-order code, DRM10; – – – –, second-order code, DRM10; —·—, fourth-order code, DSM no explicit filtering; —··—, second-order code, DSM no explicit filtering; and ——, DNS.

2001). Better representation of turbulence intensities is, for example, very important in applications where accurate prediction of turbulent mixing is required. These results therefore demonstrate that improvements can be obtained for a given resolution and code by using explicit filtering and reconstruction.

The implications of these results for LES for engineering applications must be considered carefully. For engineering flows, traditional LES (without explicit filtering) is commonly performed with the DSM using a tophat test filter. As shown in this investigation, this method poorly predicts both mean velocity profiles and turbulence intensities. There are several choices that must be made in determining how best to improve the performance of LES in practical applications.

Choosing the appropriate grid resolution for a simulation is necessarily the first step, as our results show great discrepancies among simulations with different grid sizes. Two main concerns must be addressed when selecting the necessary grid resolution. First, the grid should be able to resolve important physical characteristics of the flow. Second, the grid must also be fine enough to obtain a solution that is not greatly affected by the numerical errors.

The order of accuracy of the finite difference scheme used also greatly affects the solution. Note, for example, that the difference between the predicted mean velocity profiles for simulations using different turbulence models was larger for the fourth-order than for the second-order code. The higher sensitivity of the fourth-order code may be due to smaller numerical errors, and/or to the coarser resolution used in these simulations (compared to the resolution of the second-order code), so that the turbulence models play a larger role in the fourth-order case.

Finally, explicit filtering can be used as a means to reduce the influence of numerical errors in the high wavenumbers. Increasing the grid resolution improves the representation of the important large energy-containing scales. However, the

truncation errors in the high-wavenumber portion remain. It is precisely these high wavenumbers that are often used to represent SGS motions, and it is therefore imperative that they be represented as accurately as possible.

The extra computational cost due to explicit filtering to obtain increased accuracy may be worthwhile as LES continues to be applied to increasingly complex geometries and to problems where fine resolutions are not practical. The improvements obtained by use of the DRM10 (and the DRM5) model may be even more significant at coarser resolutions. Tests with DRM10 with the second-order code at a resolution of (48,37,36) show improvements over the DSM with the tophat filter (without explicit filtering) even with such an under-resolved simulation (not shown). The turbulence intensities predicted by DRM10 are much better than those by the DSM, even though the improvement in the mean velocity profile is small.

As this investigation has shown, the explicit filtering approach has the potential to improve simulation results. RSFS models with different levels of reconstruction were considered. The LES results with explicit filtering improve as the level of reconstruction is increased. No significant improvements were observed between DRM5 and DRM10, indicating that the reconstruction is probably adequate at level five (which is also less expensive computationally); discretization errors and poor performance of the SGS model prevent the results from further approaching the filtered DNS data. The ability of the SGS (or RSFS) model to account for such numerical errors due to the discretization and finite difference schemes is of course desirable. There is, therefore, a great need to develop SGS models that work well in the context of explicit filtering, where the accuracy of the smallest scales is increased. In addition, the effect of filtering in all three directions (and the resulting commutation errors) needs to be investigated.

Thanks are extended to Dr H. Jeanmart and Professor G. S. Winckelmans who contributed greatly through many discussions during the Center for Turbulence Research Summer Program 2002, where this research was conducted. Thanks are also due to Professors J. H. Ferziger, P. Moin, and R. L. Street for their input, as well as to Professor O. V. Vasilyev for providing the channel flow codes. The support of NSF Grant ATM-0073395 (Physical Meteorology Program: R. R. Rogers, Program Director) for F. K. C. is gratefully acknowledged.

REFERENCES

Bardina, J., Ferziger, J. & Reynolds, W. 1983 Improved turbulence models based on large eddy simulation of homogeneous, incompressible, turbulent flows. *Tech. Rep.* TF-19. Department of Mechanical Engineering, Stanford University, Stanford, California.

Carati, D., Winckelmans, G. & Jeanmart, H. 2001 On the modelling of the subgrid-scale and filtered-scale stress tensors in large-eddy simulation. *J. Fluid Mech.* **441**, 119–138.

Chow, F. & Street, R. 2002 Modelling unresolved motions in LES of field-scale flows. In *American Meteorological Society, 15th Symp. on Boundary Layers and Turbulence*, pp. 432–435.

Chow, F. K. & Moin, P. 2003 A further study of numerical errors in large-eddy simulations. *J. Comput. Phys.* **184**, 366–380.

van Cittert, P. 1931 Zum Einfluß der Spaltbreite auf die Intensitätsverteilung in Spektrallinien II. *Zeitschrift für Physik* **69**, 298.

Dukowicz, J. & Dvinsky, A. 1992 Approximate factorization as a high-order splitting for the implicit incompressible-flow equations. *J. Comput. Phys.* **102**, 336–347.

Germano, M., Piomelli, U., Moin, P. & Cabot, W. 1991 A dynamic subgrid-scale eddy viscosity model. *Phys. Fluids* **3**, 1760–1765.

Ghosal, S. 1996 An analysis of numerical errors in large-eddy simulations of turbulence. *J. Comput. Phys.* **125**, 187–206.

Ghosal, S. & Moin, P. 1995 The basic equations for the large eddy simulation of turbulent flows in complex geometry. *J. Comput. Phys.* **118**, 24–37.

Gullbrand, J. 2000 An evaluation of a conservative fourth order dns code in turbulent channel flow. *Annual Research Briefs*, pp. 211–218. Center for Turbulence Research, NASA Ames–Stanford University.

Gullbrand, J. 2001 Explicit filtering and subgrid-scale models in turbulent channel flow. *Annual Research Briefs*, pp. 31–43. Center for Turbulence Research, NASA Ames–Stanford University.

Jeanmart, H. & Winckelmans, G. 2002 Comparison of recent dynamic subgrid-scale models in the case of the turbulent channel flow. *Proc. Summer Program*, pp. 150–116. Center for Turbulence Research, NASA Ames–Stanford University.

Katopodes, F., Street, R. & Ferziger, J. 2000 A theory for the subfilter-scale model in large-eddy simulation. *Tech. Rep.* 2000-K1. Environmental Fluid Mechanics Laboratory.

Leonard, A. 1974 Energy cascade in large eddy simulations of turbulent fluid flows. *Adv. Geophys.* **18A**, 237–248.

Lilly, D. 1992 A proposed modification of the Germano subgrid-scale closure method. *Phys. Fluids* **4**, 633–635.

Lund, T. & Kaltenbach, H.-J. 1995 Experiments with explicit filtering for LES using a finite-difference method. *Annual Research Briefs*, pp. 91–105. Center for Turbulence Research, NASA Ames-Stanford University,

Lund, T. S. 1997 On the use of discrete filters for large eddy simulation. *Annual Research Briefs*, pp. 83–95. Center for Turbulence Research, NASA Ames-Stanford University.

Moin, P. 2001 *Fundamentals of Engineering Numerical Analysis*. Cambridge University Press.

Morinishi, Y., Lund, T., Vasilyev, O. & Moin, P. 1998 Fully conservative higher order finite difference schemes for incompressible flow. *J. Comput. Phys.* **143**, 90–124.

Moser, R., Kim, J. & Mansour, N. 1999 Direct numerical simulation of turbulent channel flow up to $Re_\tau = 590$. *Phys. Fluids* **11**, 943–945.

Najjar, F. & Tafti, D. 1996 Study of discrete test filters and finite difference approximations for the dynamic subgrid-scale stress model. *Phys. Fluids* **8**, 1076–1088.

Piomelli, U., Moin, P. & Ferziger, J. 1988 Model consistency in large eddy simulation of turbulent channel flows. *Phys. Fluids* **31**, 1884–1891.

Smagorinsky, J. 1963 General circulation experiments with the primitive equations. *Mon. Weath. Rev.* **91**, 99–152.

Spalart, P., Moser, R. & Rogers, M. 1991 Spectral methods for the Navier–Stokes equations with one infinite and 2 periodic directions. *J. Comput. Phys.* **96**, 297–324.

Stolz, S., Adams, N. & Kleiser, L. 2001 An approximate deconvolution model for large-eddy simulation with application to incompressible wall-bounded flows. *Phys. Fluids* **13**, 997–1015.

Vasilyev, O. 2000 High order finite difference schemes on non-uniform meshes with good conservation properties. *J. Comput. Phys.* **157**, 746–761.

Vreman, B., Geurts, B. & Kuerten, H. 1994 On the formulation of the dynamic mixed subgrid-scale model. *Phys. Fluids* **6**, 4057–4059.

Winckelmans, G. & Jeanmart, H. 2001 Assessment of some models for LES without/with explicit filtering. In *Direct and Large-Eddy Simulation IV* (ed. B. Geurts, F. Friedrich & O. Métais), pp. 55–66. Kluwer.

Winckelmans, G., Jeanmart, H. & Carati, D. 2002 On the comparison of turbulence intensities from large-eddy simulation with those from experiment or direct numerical simulation. *Phys. Fluids* **14**, 1809–1811.

Winckelmans, G., Wray, A., Vasilyev, O. & Jeanmart, H. 2001 Explicit-filtering large-eddy simulation using the tensor-diffusivity model supplemented by a dynamic smagorinsky term. *Phys. Fluids* **13**, 1385–1403.

Yeo, W. & Bedford, K. 1988 Closure-free turbulence modeling based upon a conjunctive higher order averaging procedure. In *Computational Methods in Flow Analysis* (ed. H. Niki & M. Kawahara), pp. 844–851. Okayama University of Science, Okayama.

Zhou, Y., Brasseur, J. & Juneja, A. 2001 A resolvable subfilter-scale model specific to large-eddy simulation of under-resolved turbulence. *Phys. Fluids* **13**, 2602–2610.